Title
The kinetics of selective oxidation of propene on bismuth vanadium molybdenum oxide catalysts

Authors
Zhai, Z
Getsoian, AB
Bell, AT

Publication Date
2013-06-17

DOI
10.1016/j.jcat.2013.05.008

Peer reviewed

ChemPubSoc Europe

DOI: 10.1002/celc.201701316

CHEMELECTROCHEM Articles

Effects of Anion Identity and Concentration on Electrochemical Reduction of CO_2

Joaquin Resasco,[a, c] Yanwei Lum,[b, c] Ezra Clark,[a, c] Jose Zamora Zeledon,[a, c] and Alexis T. Bell*[a, c]

The electrochemical reduction of CO_2 is known to be influenced by the concentration and identity of the anionic species in the electrolyte; however, a full understanding of this phenomenon has not been developed. Here, we present the results of experimental and computational studies aimed at understanding the role of electrolyte anions on the reduction of CO_2 over Cu surfaces. Experimental studies were performed to show the effects of bicarbonate buffer concentration and the composition of other buffering anions on the partial currents of the major products formed by reduction of CO_2 over Cu. It was demonstrated that the composition and concentration of electrolyte anions has relatively little effect on the formation of CO, $HCOO^-$, C_2H_4, and CH_3CH_2OH, but has a significant effect on the formation of H_2 and CH_4. Continuum modeling was used to assess the effects of buffering anions on the pH at the electrode surface. The influence of pH on the activity of Cu for producing H_2 and CH_4 was also considered. Changes in the pH near the electrode surface were insufficient to explain the differences in activity and selectivity observed with changes in anion buffering capacity observed for the formation of H_2 and CH_4. Therefore, it is proposed that these differences are the result of the ability of buffering anions to donate hydrogen directly to the electrode surface and in competition with water. The effectiveness of buffering anions to serve as hydrogen donors is found to increase with decreasing pK_a of the buffering anion.

1. Introduction

The electrochemical reduction of CO_2 offers a means for storing electrical energy produced by intermittent renewable resources, such as wind and solar radiation.[1,2] Hydrocarbons and alcohols are the preferred products of the CO_2 reduction reaction (CO2RR) because of their high energy density. To date, the only electrocatalyst that can produce these products with significant yields is copper (Cu).[3–5] While a large fraction of the total current used for the CO2RR over Cu yields desirable products, such as ethylene (C_2H_4) and ethanol (CH_3CH_2OH), a significant fraction of the total current goes to producing undesired products, such as hydrogen (H_2), methane (CH_4), carbon monoxide (CO), and formate anions ($HCOO^-$).[6,7] Since H_2 is the largest component of the undesired products, it is desirable to identify means for enhancing the fraction of the total current use to produce desired products of CO_2 reduction by mitigating the production of H_2. To do so requires understanding of how the composition and concentration of the electrolyte influence the mechanism of the CO2RR. We have previously demonstrated that alkali metal cations influence the distribution of products formed as a consequence of electrostatic interactions between solvated cations present at the outer Helmholtz plane and adsorbed species on the cathode surface that have large dipole moments (e.g., $*CO_2$, *CO, *OCCO).[8] This field stabilization decreases the energy for $*CO_2$ adsorption, the precursor to two-electron products, and C-C coupling to form *OCCO or *OCCHO, the precursor to C_2H_4 and C_2H_5OH.[8] As a consequence, the partial currents for forming H_2 and CH_4 are unaffected by the size of the alkali metal cation (Li^+ through Cs^+), whereas the partial currents for forming $HCOO^-$, C_2H_4, and CH_3CH_2OH increase monotonically with increasing alkali metal cation size.

A number of studies have also shown the distribution of products formed by CO_2 reduction over Cu is influenced by changes in the composition of the electrolyte anions.[7–9] Hori and coworkers have demonstrated that non-buffering anions (Cl^-,ClO_4^-, SO_4^{2-}) give high selectivities to C_2H_4 and CH_3CH_2OH, and lower selectivity to CH_4 and H_2 compared to bicarbonate anions (HCO_3^-), whereas phosphate anions ($H_2PO_4^-$) result in a higher selectivity to H_2 and CH_4.[7] The effects of bicarbonate concentration have also been investigated, and it has been reported that with increasing anion concentration the rates of hydrogen evolution and methane production increased.[7,9,10] The observed differences in selectivity with buffer concentration and buffer capacity were attributed to changes in the pH at the electrode surface; however, these changes in pH were not quantified nor was it explained how the electrolyte pH

[a] Dr. J. Resasco, E. Clark, J. Z. Zeledon, Prof. A. T. Bell
Department of Chemical Engineering,
University of California,
Berkeley, CA 94720
E-mail: alexbell@berkeley.edu
[b] Y. Lum
Department of Materials Science and Engineering,
University of California,
Berkeley, CA 94720
[c] Dr. J. Resasco, Y. Lum, E. Clark, J. Z. Zeledon, Prof. A. T. Bell
Joint Center for Artificial Photosynthesis,
Material Science Division,
Lawrence Berkeley National Laboratory,
Berkeley, CA 94720

Supporting information for this article is available on the WWW under https://doi.org/10.1002/celc.201701316

might cause the observed changes in product distribution.[7,9,10] Recent studies have also discussed the possibility of HCO_3^- acting as a carbon source.[11–13] Given the lack of a clear interpretation of the effects of anion composition on the activity and selectivity of Cu for the CO_2RR, we undertook an effort to develop a complete picture of the role of anionic species on the electrochemical reduction of CO_2. Our studies show that changes in pH in the vicinity of the electrode surface are insufficient to explain the differences in activity and selectivity observed with changes in anion buffering capacity, and we propose that these differences are the result of the ability of buffering anions to donate hydrogen directly to the electrode surface.

Experimental Section

Electrode Preparation

Cu thin films with specific crystal orientations were prepared by rf sputtering of Cu onto silicon (Si) single crystal substrates. This approach is based on previous studies demonstrating the epitaxial relationship between Cu and Si substrates of different orientations.[8,14,15] Cu(100)-oriented thin films were used for the present study because it has been shown that this surface exhibits a high selectivity to the desired C_{2+} hydrocarbons and oxygenates (e.g., C_2H_4 and CH_3CH_2OH) and has been shown to be electrochemically stable.[16] Single-side polished Si(100) wafers (Virginia semiconductor, 1–10 Ω cm) were diced into ~4 cm^2 sized pieces that were then used as electrode substrates. Prior to Cu deposition, the native oxide was removed from the Si substrates by submerging them in a 10% HF solution for 5 min. Immediately after HF etching, the Si pieces were transferred to a vacuum chamber for sputter deposition of Cu in an AJA ATC Orion-5 sputtering system. The base pressure of the sputtering system prior to deposition was $\sim 2\times10^{-7}$ Torr. The flow rate of the sputtering gas (Ar) was 25 sccm and the sputtering pressure was adjusted to 2×10^{-3} Torr by controlling the speed at which the chamber was pumped, using a variable butterfly valve. Cu (99.999% Kurt Lesker) was deposited at a rate of 1 Å/s, as determined by a calibrated quartz crystal monitor, at ambient temperature. The total film thickness deposited was 100 nm.

Electrode Characterization

The structure of the Cu thin films was characterized by X-ray diffraction. The orientation and epitaxial quality of the films were determined using symmetric θ–2θ scans, in plane ϕ scans, ω scans or rocking curves, and pole figures. XRD patterns were taken with a PANanalytical X'Pert diffractometer, which uses a Cu Kα ($\lambda =$ 1.54056 Å) X-ray source. Symmetric θ–2θ scans were collected on samples fixed onto a flat glass slide in locked-coupled mode with a goniometer resolution of 0.001°. Measured diffraction patterns were compared to known standards taken from the International Center for Diffraction Data (ICDD) PDF4 database (card #71-4610 for Cu). X-ray diffraction analysis using both in plane and out of plane techniques demonstrate that Cu thin films can be grown epitaxially with in the (100) orientation from Si(100) (Supporting Information).[8]

Electrolyte Preparation

Electrolyte solutions were prepared by mixing ultra-pure salts and 18.2 MΩ DI, and were used as the electrolyte without further purification. Bicarbonate buffered electrolytes were prepared from K_2CO_3 (99.995% Sigma Aldrich) which upon saturation gave $KHCO_3$ electrolytes of concentrations of 0.05, 0.10, and 0.20 M. To maintain constant salinity, K_2SO_4 (Sigma Aldrich 99.99%) was added to these solutions to a total salinity of 0.2 M. The pH of these solutions after CO_2 saturation was 6.4, 6.8, and 7.0 respectively. Phosphate buffered electrolytes were prepared from 0.05 M KH_2PO_4 (Sigma Aldrich 99.99%) and 0.05 M K_2HPO_4 (Sigma Aldrich 99.99%). The pH of this solution after CO_2 saturation was 6.8. Borate buffered electrolyte was prepared from 0.05 M $K_2B_4O_7$ (Sigma Aldrich 99.9%). The pH of this solution after CO_2 saturation was 6.7. Unbuffered solutions were prepared from 0.05 M K_2SO_4 and 0.1 M $KClO_4$ (Sigma Aldrich 99.99%). The pH's of these solutions after CO_2 saturation were 4.5 and 4.0 respectively.

Electrochemical Measurements

All electrochemical experiments were conducted in a gas-tight electrochemical cell machined from polyether ether ketone (PEEK).[17] The cell was cleaned with 20 wt.% nitric acid and oxidized in UV-generated ozone for 15 min prior to the initiation of an experiment. The working and counter electrodes were parallel and separated by an anion-conducting membrane (Selemion AMV AGC Inc.). A gas dispersion frit was incorporated into the cathode chamber to provide vigorous electrolyte mixing. The exposed geometric surface area of each electrode was 1 cm^2 and the electrolyte volume of each electrode chamber was 1.8 mL. The counter electrode was a Pt foil (99.9% Sigma Aldrich) that was flame annealed prior to each experiment. The working electrode potential was referenced against an Ag/AgCl electrode (Innovative Instruments Inc.) that was calibrated against a homemade standard hydrogen electrode (SHE). The cathode chamber was sparged with CO_2 (99.999% Praxair) at a rate of 5 sccm for 20 min prior to and throughout the duration of all electrochemical measurements.

Electrochemical measurements were performed using a Biologic VSP-300 potentiostat. All electrochemical data were recorded versus the reference electrode and converted to the RHE scale. Potentiostatic electrochemical impedance spectroscopy (PEIS) was used to determine the uncompensated resistance (R_u) of the electrochemical cell by applying voltage waveforms about the open circuit potential with an amplitude of 20 mV and frequencies ranging from 50 Hz to 500 kHz. The potentiostat compensated for 85% of R_u *in situ* and the last 15% was post-corrected to arrive at accurate potentials. The electrocatalytic activity was assessed by conducting chronoamperometry at each fixed applied potential for 70 min.

Product Analysis

The effluent from the electrochemical cell was passed through the sampling loop (250 μL) of an Agilent 7890B gas chromatograph equipped with a pulsed-discharge helium ionization detector (PDHID). He (99.9999% Praxair) was used as the carrier gas. The effluent of the electrochemical cell was sampled every 14 min. The gaseous products were separated using a Hayesep-Q capillary column (Agilent) connected in series with a packed ShinCarbon ST column (Restek Co.). The column oven was maintained at 50 °C for 1 min followed by a temperature ramp at 30 °C/min to 250 °C, which was maintained for the duration of the analysis. The signal response of the PDHID to each gaseous product was calibrated by analyzing a series of NIST-traceable standard gas mixtures (Air Gas).

The electrolyte from both electrode chambers was collected after electrolysis and analyzed using a Thermo Scientific UltiMate 3000 liquid chromatograph equipped with a refractive index detector (RID). The electrolyte aliquots were stored in a refrigerated

autosampler until analyzed in order to minimize the evaporation of volatile products. The liquid-phase products contained in a 10 μL sample were separated using a series of two Aminex HPX 87-H columns (Bio-Rad) and a 1 mM sulfuric acid eluent (99.999% Sigma Aldrich). The column oven was maintained at 60 °C for the duration of the analysis. The signal response of the RID to each liquid-phase product was calibrated by analyzing standard solutions of each product at a concentration of 1, 10, and 50 mM.

Numerical Simulations

To understand the effects of transport phenomena on the measured rates of CO_2 reduction, we used a diffusion-reaction model based on the work of Gupta et al. to determine the pH and buffering anion concentration at the cathode.[18] We can consider the bulk of the electrolyte to be a well-mixed solution with concentrations of all species to be at their equilibrium values. This assumption is based on the vigorous agitation of the electrolyte by a stream of bubbles of CO_2. We assume that near the cathode surface there is a mass transfer boundary layer within which concentrations of each species change from that in the bulk to that at the cathode surface. CO_2 will diffuse through this boundary layer towards the electrode surface while hydroxide ions will diffuse away from the surface. Simultaneously, acid-base reactions consume and generate these species in the boundary layer, while CO_2 is consumed and OH^- is produced at the electrode surface. The reactions governing the acid base equilibria for bicarbonate electrolytes are shown below [Eqs. (1)–(3)]:

$$CO_{2(g)} \leftrightarrow CO_{2(aq)} \quad (1)$$

$$CO_{2(aq)} + OH^-_{(aq)} \leftrightarrow HCO^-_{3(aq)} \quad (2)$$

$$HCO^-_{3(aq)} + OH^-_{(aq)} \leftrightarrow CO^{2-}_{3(aq)} + H_2O_{(l)} \quad (3)$$

Dissolved CO_2 can also be hydrated to form carbonic acid; however, its concentration is $\sim 10^{-3}$ of the concentration of dissolved CO_2. Therefore, the hydrated and dissolved CO_2 may be considered as a single species.[19] The associated rate and equilibrium constants for these reactions are taken from previous literature reports:[19–21] $K_1 = 3.35x10^{-2}$ M atm^{-1}, $K_2 = 4.44x10^7$ M^{-1}, $k_{2f} = 5.93x10^3$ M^{-1} s^{-1}, $k_{2r} = 1.34x10^{-4}$ s^{-1}, $K_3 = 4.66x10^3$ M^{-1}, $k_{3f} = 1.00x10^8$ M^{-1} s^{-1}, $k_{2r} = 2.15x10^4$ s^{-1}. For the case in which biphosphate anion are used, the following acid-base reactions must be included [Eqs. (4)–(6)]:

$$H_3PO_{4(aq)} + OH^-_{(aq)} \leftrightarrow H_2PO^-_{4(aq)} + H_2O_{(l)} \quad (4)$$

$$H_2PO^-_{4(aq)} + OH^-_{(aq)} \leftrightarrow HPO^{2-}_{4(aq)} + H_2 \quad (5)$$

$$HPO^{2-}_{4(aq)} + OH^-_{(aq)} \leftrightarrow PO^{3-}_{4(aq)} + H_2O_{(l)} \quad (6)$$

The equilibrium constants for these reactions are taken from previous literature reports:[20] $K_4 = 6.92\ x\ 10^{11}\ M^{-1}$, $K_5 = 6.17x10^6\ M^{-1}$, $K_6 = 4.79x10^1\ M^{-1}$.

The concentrations of the relevant species at different reaction conditions are governed by the following set of coupled partial differential equations, which account for the simultaneous diffusion and reaction of all species but neglect their migration [Eqs. (7)–(10)]:

$$\frac{\partial(CO_{2(aq)})}{\partial t} = D_{CO_{2(aq)}} \frac{\partial^2(CO_{2(aq)})}{\partial x^2} - k_{2f}(CO_{2(aq)})\left(OH^-_{(aq)}\right) + k_{2r}\left(HCO^-_{3(aq)}\right) \quad (7)$$

$$\frac{\partial\left(HCO^-_{3(aq)}\right)}{\partial t} = D_{HCO^-_{3(aq)}} \frac{\partial^2\left(HCO^-_{3(aq)}\right)}{\partial x^2} + k_{2f}(CO_{2(aq)})\left(OH^-_{(aq)}\right) - k_{2r}\left(HCO^-_{3(aq)}\right) - k_{3f}\left(HCO^-_{3(aq)}\right)\left(OH^-_{(aq)}\right) + k_{3r}\left(CO^{2-}_{3(aq)}\right) \quad (8)$$

$$\frac{\partial\left(CO^{2-}_{3(aq)}\right)}{\partial t} = D_{CO^{2-}_{3(aq)}} \frac{\partial^2\left(CO^{2-}_{3(aq)}\right)}{\partial x^2} + k_{3f}\left(HCO^-_{3(aq)}\right)\left(OH^-_{(aq)}\right) - k_{3r}\left(CO^{2-}_{3(aq)}\right) \quad (9)$$

$$\frac{\partial\left(OH^-_{(aq)}\right)}{\partial t} = D_{OH^-_{(aq)}} \frac{\partial^2\left(OH^-_{(aq)}\right)}{\partial x^2} - k_{2f}(CO_{2(aq)})\left(OH^-_{(aq)}\right) + k_{2r}\left(HCO^-_{3(aq)}\right) - k_{3f}\left(HCO^-_{3(aq)}\right)\left(OH^-_{(aq)}\right) + k_{3r}\left(CO^{2-}_{3(aq)}\right) \quad (10)$$

The boundary conditions for Eqs. (7)–(10) are set at the electrode surface ($x = 0$) and at the edge of the boundary layer ($x = \delta$). A boundary layer thickness of 100 μm was assumed. This value is comparable to that measured previously under the same flow conditions in the electrochemical cell used for the present studies.[22] At the edge of the boundary layer, the concentrations of all species are set to their bulk equilibrium values and at the electrode surface, the experimentally measured data give the rates of CO_2 consumption and OH^- generation [Eqs. (11)–(14)]:

$$D_{CO_{2(aq)}} \frac{d(CO_{2(aq)})}{\partial x} = R_{CO2} \quad (11)$$

$$D_{HCO^-_{3(aq)}} \frac{d\left(HCO^-_{3(aq)}\right)}{\partial x} = 0 \quad (12)$$

$$D_{CO^{2-}_{3(aq)}} \frac{d\left(CO^{2-}_{3(aq)}\right)}{\partial x} = 0 \quad (13)$$

$$D_{OH^-_{(aq)}} \frac{d\left(OH^-_{(aq)}\right)}{\partial x} = R_{OH-} \quad (14)$$

Here, R_{CO2} and R_{OH-} are the rates of CO_2 consumption and hydroxide generation, respectively, in units of moles/s cm^2. Diffusion coefficients were taken from previous data:[20] $D_{CO_{2(aq)}} = 1.91\times10^{-9}$ m^2 s^{-1}, $D_{HCO^-_{3(aq)}} = 9.23\times10^{-10}$ m^2 s^{-1}, $D_{CO^{2-}_{3(aq)}} = 1.19\times10^{-9}$ m^2 s^{-1}, $D_{OH^-_{(aq)}} = 5.27\times10^{-9}$ m^2 s^{-1}. Eqs. (7)–(10) together with the boundary conditions given by Eqs. (11–14) were solved using COMSOL Multiphysics 5.1 to yield pH and CO_2 concentration profiles in the hydrodynamic boundary layer.

2. Results and Discussion

The steady-state activity and selectivity of the Cu(100) surface were investigated by potentiometric electrolysis at potentials between −0.7 and −1.0 V vs. the reversible hydrogen electrode (RHE). The initial measurements were carried out in CO_2-

saturated electrolytes of 0.05 M, 0.10 M, and 0.20 M $KHCO_3$ with K_2SO_4 added to maintain the salinity of each electrolyte at 0.2 M. Figure 1 shows that with increasing buffer concentration, the partial currents of H_2 and CH_4 formation increase. By contrast, the partial currents of CO, $HCOO^-$, C_2H_4 and CH_3CH_2OH formation are minimally affected by buffer concentration, when the cathode voltage is given versus the standard hydrogen electrode (SHE), which accounts for differences in bulk pH of the electrolyte. These results are consistent with previous studies on the effects of bicarbonate concentration on the activity of Cu for the CO2RR.[7,9,10,23]

To understand why it the partial currents of H_2 and CH_4 should be plotted on the RHE scale and those for the CO, $HCOO^-$, C_2H_4, and CH_3CH_2OH on the SHE scale, it is necessary to review the meaning of these scales and understand how they relate to the elementary processes leading to each product. The SHE scale defines the potential for a given reaction relative to the potential for the reaction [Eq. (15)]:

$$2\ H^+_{(aq)} + 2\ e^- \leftrightarrow\ H_{2(g)} \tag{15}$$

with all components at unit activity ($P_{H_2} = 1$ bar, $a_{H^+} = 1$), the reference state. For these conditions, the potential for reaction 1 is $E^o_{H_2}$, which by convention is set to zero. The potential of the standard hydrogen electrode can be determined for other conditions using the Nernst equation [Eq. (16)]:

$$E_{H_2} = E^o_{H_2} + \frac{RT}{2F} \ln \frac{[H^+]}{p^{1/2}_{H_2}} \tag{16}$$

At room temperature and fixed pressure of hydrogen ($P_{H_2} = 1$ bar), Equation (16) reduces to Equation (17):

$$E_{H_2} = E^o_{H_2} - 0.059\ pH \tag{17}$$

The potential for any chemical reaction can now be referenced to the SHE and is given by Equation (18):

$$E_{SHE} = E^o_{SHE} - 0.059\ pH \tag{18}$$

Here E^o_{SHE} is the potential for the reaction of interest referenced to the standard hydrogen electrode under standard conditions.

A second reference potential scale is the reversible hydrogen electrode scale (RHE). The reversible hydrogen electrode is a subtype of the standard hydrogen electrode and is used for electrochemical processes. Unlike the standard hydrogen electrode, potentials measured relative to the reference hydrogen electrode do not change with pH. The RHE scale and the SHE scale are related by Equation (19):

$$E_{RHE} = E_{SHE} + 0.059\ pH \tag{19}$$

For reactions involving the same number of protons and electrons, the partial current vs. cathode potential expressed on

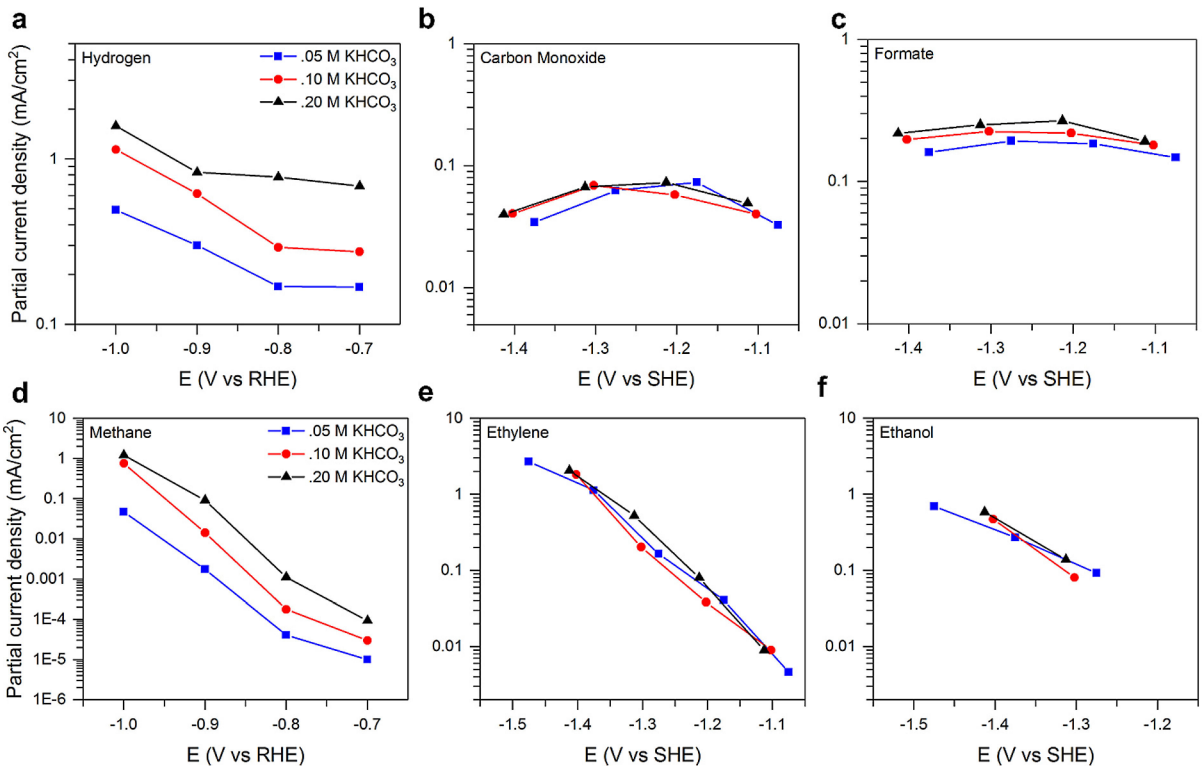

Figure 1. Effect of bicarbonate buffer concentration on the partial currents of formation of major products of CO_2 reduction over Cu(100). Partial current densities for each of the major products as a function of the bicarbonate buffer concentration on Cu(100). Data are presented at potential between −0.7 and −1.0 V vs. RHE. For C_2H_4 and CH_3CH_2OH, partial currents are reported against an SHE scale.

the RHE scale is not expected to shift with pH. An example of such a reaction would be the hydrogenation of adsorbed CO [Eq. (20)]:

$$^{*}CO + H^{+} + e^{-} \rightarrow {}^{*}CHO \quad (20)$$

However, if the reaction does not involve a proton-electron transfer, the partial current vs. cathode potential expressed on SHE scale should not shift with pH. An example of a reaction of this type is the coupling of two adsorbed CO molecules [Eq. (21)]:

$$^{*}CO + {}^{*}CO \rightarrow {}^{*}OCCO \quad (21)$$

It should be noted that these conclusions will hold under conditions, such as those relevant to the CO2RR, where electron reduction of water, $H_2O + e^- \rightarrow \frac{1}{2}H_{2(g)} + OH^-_{(aq)}$, rather than the reduction of a proton, $H^+_{(aq)} + e^- \leftrightarrow \frac{1}{2}H_{2(g)}$, is the principal source of hydrogen. We note that a proton transfer reaction in which water is the reactant depends on pH in the same was as if a proton were the reactant, since the concentrations of protons and hydroxide ions are related through the following relationship [Eq. (22)]:

$$-\log[H^+] - \log[OH^-] = 14 \quad (22)$$

It has been observed previously that partial currents for the formation of multi-carbon products such as C_2H_4 and CH_3CH_2OH are pH independent when the cathode potential is reported on an SHE scale, meaning that they are sensitive to pH on an RHE scale.[23] In particular, the potential at which these products are observed becomes more positive as the pH of the electrolyte increases, in accordance with the Nernst equation. This conclusion can be understood considering the mechanism for the formation of these products. Density functional theory calculations have shown that carbon-carbon bond formation is the rate determining step for forming any multi-carbon product observed during CO_2R.[24,25] and occurs via coupling of two adsorbed CO molecules (denoted *CO) or the addition of an adsorbed CO molecule to an adsorbed formyl (*CHO) molecule [Eqs. (23) and (24)]:

$$^{*}CO + {}^{*}CO \rightarrow {}^{*}OCCO \quad (23)$$

$$^{*}CO + {}^{*}CHO \rightarrow {}^{*}OCCHO \quad (24)$$

Since neither of these elementary reactions involves a proton transfer in the rate determining step, the rates of both reactions should be pH independent, consistent with the observation of a pH independence of the rate of multi-carbon product formation on an SHE scale. Therefore, our observation (see Figure 1) that the partial currents for the formation of C_2H_4 and CH_3CH_2OH formation are independent of buffer concentration when the rates are compared on an SHE scale is what should be expected. Similarly, the production of CO and $HCOO^-$ have previously been shown to be independent of pH, suggesting that the rate limiting step does not involve a concerted proton-coupled electron-transfer step, but rather electron transfer to form a $CO_2^{\delta-}$.[13,26–29] We note here that the effects of pH and buffer concentration on the formation of CO and $HCOO^-$ can be observed more readily on metals selective for these products.

The rate limiting step for production of methane, however, is proposed to be the hydrogenation of adsorbed CO to form adsorbed CHO [Eq. (25)].[30]

$$^{*}CO + H_2O + e^- \rightarrow {}^{*}CHO + OH^- \quad (25)$$

Consequently, this reaction should have a pH dependence on an SHE scale, and be pH independent on an RHE scale if no specific effects of pH are involved. Similarly, hydrogen evolution should be pH independent on an RHE scale assuming no explicit effects of pH.

For the data presented in Figure 1, the cathode potential on the RHE scale was determined using the bulk pH of the solution. Previous work has shown that while the bulk of CO_2-saturated electrolyte solution of $KHCO_3$ has a pH of 6.8, the pH near the cathode can rise to nearly 10, as a consequence of electrolyte polarization, a phenomenon that becomes particularly important for cathodes potentials below ~−0.9 V.[31] For this range of pH's, the source of hydrogen for the formation of H_2 and the hydrogenation of CO_2 is adsorbed H_2O. H atoms are produced at the cathode surface by the reaction of adsorbed H_2O with an electron. The counter product of this reaction is an OH^- anion, which is released into the electrolyte. In the presence of a buffering anion, such as HCO_3^-, the following reaction can occur [Eq. (26)]:

$$OH^- + HCO_3^- \rightarrow H_2O + CO_3^{2-} \quad (26)$$

Hydroxide anions can also react with CO_2 to form bicarbonate anions, thereby depleting the availability of the reactant. To clearly define the extent to which the pH at the cathode surface affects partial current densities for H_2 and CH_4, the surface pH was calculated as a function of the current density for different HCO_3^- concentrations (see Methods for full description).[18,31]

Figure 2 shows that the pH at the cathode surface is higher than that of the bulk electrolyte, and increases with increasing current density as a consequence of the increase in the rate of hydroxide anion formation at the cathode. However, the differences in surface pH with buffer concentration are relatively small, particularly at low current densities, consistent with previous calculations of the effects of buffer concentration on the local pH during CO_2R.[18,31] The partial currents of H_2 and CH_4 production can now be examined on a calculated RHE scale. The calculated RHE is related to the SHE potential and the pH at the electrode surface obtained from the model, rather than the bulk electrolyte pH [Eq. (27)]:

$$E_{RHE_{calc}} = E_{SHE} + 0.059\ pH_{calc} \quad (27)$$

Figure 2 shows that substantial differences in activity persist even after differences in surface pH with buffer concentration are taken into account. Namely, the partial currents of H_2 and CH_4 production increase with buffer concentration irrespective of differences in local pH.

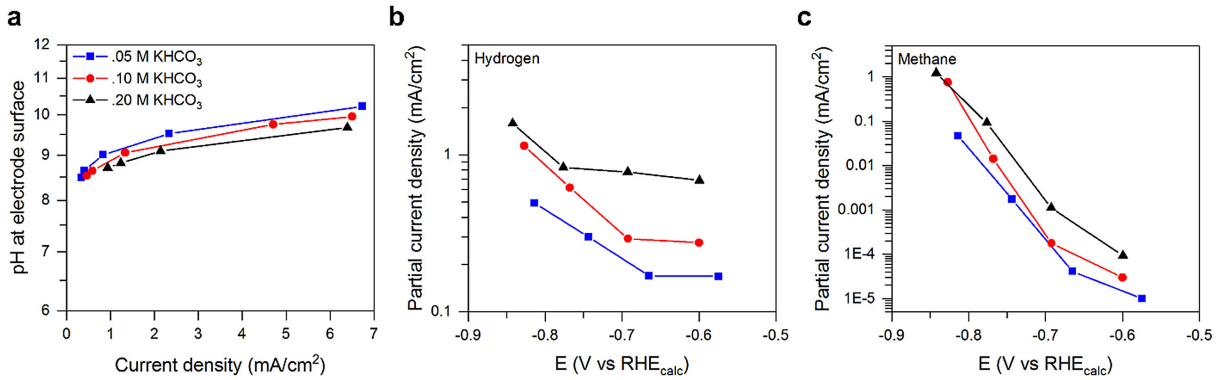

Figure 2. Surface pH effects on the partial currents of formation of major products of CO_2 reduction over Cu(100). a) pH at the electrode surface as a function of current density with increasing bicarbonate buffer concentration. b) Partial current densities for H_2 and CH_4 production as a function of the bicarbonate buffer concentration on Cu(100). Data are presented at potentials vs. RHE_{calc} using the calculated local pH, rather than the pH of the bulk electrolyte.

Previous studies have shown that HER activity is influenced by pH, contrary to what would be expected.[32–35] To investigate the influence of this effect, HER activity measurements were performed on a polycrystalline Cu electrode in a rotating disk electrode configuration in order to minimize mass transfer effects. The activity was measured as a function of electrolyte pH in the absence of CO_2 in a mixture of KCl and KOH electrolytes in order to maintain the total salinity of the electrolyte constant. Figure 3 shows that for a current density of 2.5 mA/cm^2, the overpotential for hydrogen evolution decreases with increasing electrolyte pH. This finding is consistent with previous studies of the explicit effect of pH on the rate of hydrogen evolution, and is attributed to stronger adsorption of hydrogen atoms on the surface of Cu with increasing pH.[36] The authors of this study explain that since Cu binds hydrogen more weakly than would be optimal for high HER activity, an increase in the hydrogen binding energy should increase the HER activity.[37] Therefore, the explicit effect of pH on HER activity is to increase the rate of this reaction with increasing pH. One might similarly expect the rate of methane formation to increase with increasing pH, since the rate-limiting step for this reaction has been proposed to be $*H + *CO \rightarrow *HCO$.[30,38] Figure 4 shows data, adapted from Hori and coworkers, for the partial currents of methane production from CO reduction, at a range of electrolyte pH values.[20] Similar studies for CO_2 reduction are not possible since OH^- will react with CO_2 to form HCO_3^-. These data shows that the partial current of methane formation increases with increasing pH, in a manner similar to that seen for hydrogen evolution. It is notable, though, that the trends in the rates of H_2 and CH_4 production seen in Figures 3 and 4 are opposite to those observed with increasing buffer concentration seen in Figure 1. The latter figure shows that the highest activity is observed for the highest buffer concentration, for which the near-surface pH is lowest. What we conclude from the analysis to this point is that changes in local pH with buffer concentration do not fully account for the observed differences in the rates of H_2 and CH_4 formation seen in Figure 2.

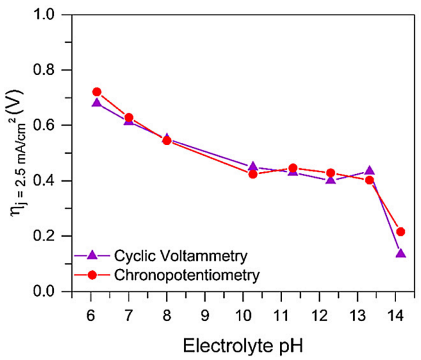

Figure 3. The overpotential for the HER over polycrystalline Cu as a function of pH for a current density of 2.5 mA/cm^2.

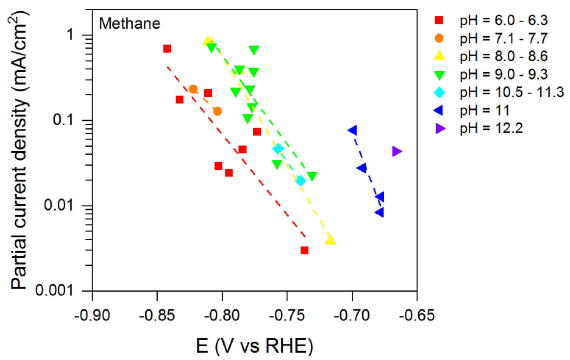

Figure 4. pH effects on the partial currents of formation of methane during CO reduction over polycrystalline Cu (adapted from Hori and co-workers).[23] Partial current densities for methane at a range of pH values. Methane activity is observed to increase with pH.

The preceding conclusion led us to examine the hypothesis that products for which the rate-limiting step involves hydrogen addition (H_2 and CH_4) should depend on the source of hydrogen, while products for which the rate-limiting step does not involve hydrogen addition should be unaffected by the nature of the source of hydrogen. A plausible explanation for the trends in partial current density observed with buffer concentration is that the hydrogen for these reaction steps may come not only from water (e.g., $H_2O + e^- \rightarrow {}^*H + OH^-$) but also from another source, such as HCO_3^- [Eq. (28)]:

$$HCO_3^- + e^- \rightarrow {}^*H + CO_3^{2-} \quad (28)$$

While this idea has been proposed previously, little evidence for it has been given.[29,39] We note that even though the concentration of HCO_3^- is substantially lower than that of water, the pK_a of HCO_3^- is 4 pK_a units lower than that of water, which means that HCO_3^- can be considered as a relevant hydrogen donor. For the case of HCO_3^-, the concentration of this anion near the cathode surface under the conditions used in the present studies is estimated to be ~50% of the bulk electrolyte concentration (0.1 M) (see SI), which is about 10^3 lower than the concentration of water (55 M). On the other hand the equilibrium constant for the deprotonation of HCO_3^- is 10^4 higher than that for H_2O. Therefore, it is conceivable that HCO_3^- could serve as a source of H atoms.

To investigate the possibility that buffering anions can act a source of hydrogen, the steady state activity and selectivity of the Cu (100) surface were investigated by potentiometric electrolysis at potentials from −0.7 to −1.0 V vs. RHE carried out in CO_2-saturated potassium-based electrolytes containing different anions. Two types of anions were used: buffering and non-buffering. For non-buffering electrolytes, the two anions chosen were perchlorate (ClO_4^-), which is a weakly adsorbing anion and sulfate (SO_4^{2-}), which is a more strongly adsorbing anion.[40] The buffering anions were chosen to have a range of pK_a's from 7 to 10. The buffer equilibrium reaction and the pK_a for each anion are shown below [Eqs. (29)–(31)]:[20]

$$HCO_3^- \leftrightarrow H^+ + CO_3^{2-}, \ \text{pKa} = 10.33 \quad (29)$$

$$B(OH)_3 + H_2O \leftrightarrow H^+ + B(OH)_4^-, \ \text{pKa} = 9.23 \quad (30)$$

$$H_2PO_4^- \leftrightarrow H^+ + HPO_4^{2-}, \ \text{pKa} = 7.21 \quad (31)$$

Figure 5 shows the partial current density of each of the major products of CO_2 reduction over Cu(100) as a function of the potential for all five electrolyte compositions. The current density for hydrogen evolution is the same for $KClO_4$ and K_2SO_4, indicating that ClO_4^- and SO_4^{2-} have no effect on the rate of the HER. Because the potentials applied during CO_2 reduction are much more negative than the potential of zero charge (PZC) of the low-index facets of Cu, ~−0.7 V_{SHE},[41] solvated cations, rather than anions should accumulate near the surface of the electrode during reaction.[24,27] On the other hand, Figure 5 shows that electrolytes containing buffering anions yield significantly higher rate of hydrogen evolution, and that the partial current increases in the order $HCO_3^- < H_3BO_3 < HPO_4^{2-}$, in the order of decreasing pK_a of the anion. The partial current for methane production is also independent of anion identity for non-buffering anions, but increases with decreasing pK_a of the buffering anion. The partial currents of CO and $HCOO^-$ formation are insensitive to the anion identity when compared on an SHE scale, and have been shown previously to be independent of pH.[26–29] The partial currents for C_2H_4 and CH_3CH_2OH vs. cathode potential expressed on the SHE scale is also independent of anion identity, consistent with previous observation.[23]

To assess the extent to which differences in the partial currents for H_2 and CH_4 observed for buffering and non-

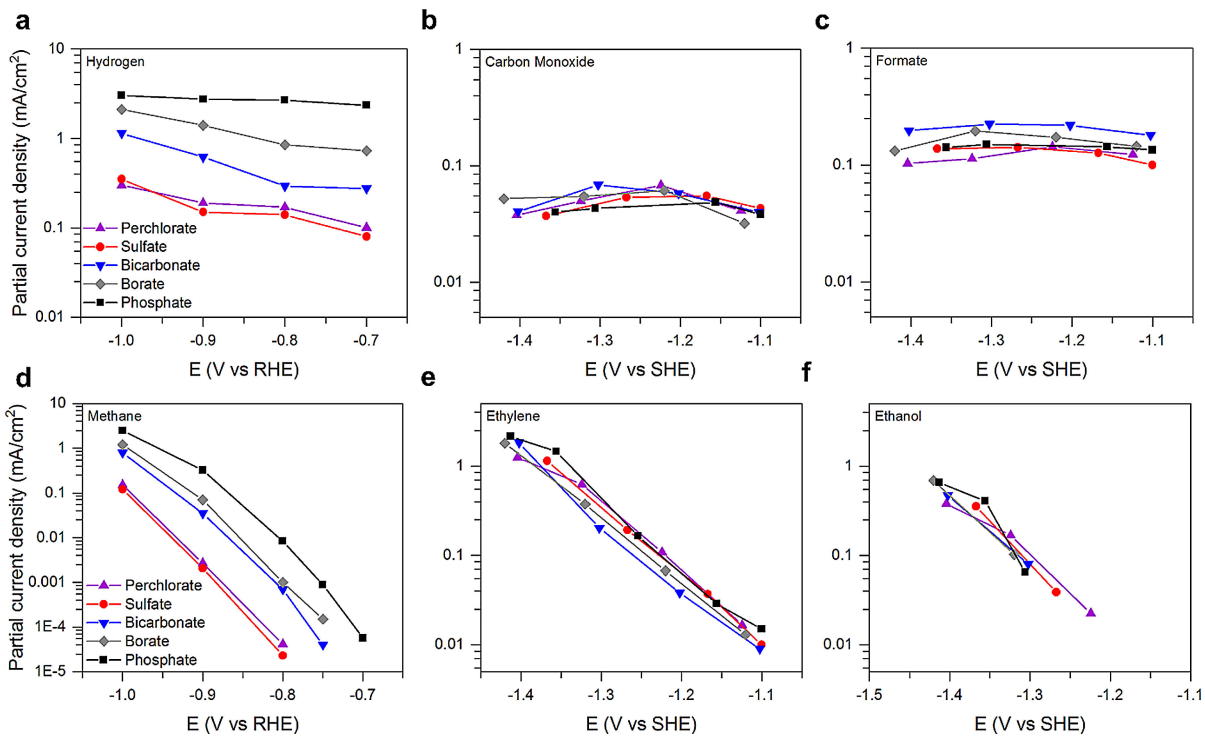

Figure 5. Partial current densities for major products of CO_2 reduction over Cu (100) in different anionic electrolytes. Partial current densities for each of the major products as a function of the electrolyte anion on Cu(100). All electrolytes are of a fixed potassium cation concentration of 0.1 M. Data are presented at potential between −0.7 and −1.0 V vs. RHE. For C_2H_4 and CH_3CH_2OH, partial currents are reported against an SHE scale.

buffering anions are due to differences in the local pH at the cathode surface, we calculated the local pH as a function of current density for all electrolytes. Figure 6a show that for non-buffering anions, the surface pH is higher than that for bicarbonate anions at any concentration. To determine whether differences in local pH could account for the differences in the observed activity, the partial currents for H_2 and CH_4 production were plotted versus the calculated RHE potential. Figures 6b and 6c shows nearly identical partial currents for H_2 and CH_4 formation in electrolyte containing ClO_4^-, SO_4^{2-}, or HCO_3^-. It is also notable that the difference between partial currents at a given cathode voltage for experiments carried out in electrolytes containing $KHCO_3$ vs. $KClO_4$ or KSO_4 is much smaller in Figure 6b than in Figure 5, suggesting that a large part of the difference seen Figure 5 is due to the differences in the pH of the electrolytes at the cathode surface. In unbuffered electrolyte, HCO_3^- can be formed from reaction of CO_2 with OH^-, and HCO_3^- could then act as a hydrogen source. However, the concentration of these anions formed is estimated to be three orders of magnitude lower than their concentration in the electrolyte with HCO_3^- intentionally added. The reason for the higher than expected partial currents of HER and methane production is likely due to the more alkaline pH near the electrode surface relative to the case in which buffers are added to the electrolyte. With increasing pH, we showed above that the HER rate increases on an RHE scale, as does the rate of methane production. Thus, HCO_3^- and H_2O at this higher pH are competitive hydrogen donors. Figure 6a shows that the cathode surface pH in KH_2PO_4 is lower than that in $KHCO_3$; however, Figure 6b shows that the partial current for H_2 is much higher in KH_2PO_4 than in $KHCO_3$. We hypothesize that this difference is due to the significantly higher ability of H_2PO4^- to serve as a source of hydrogen due to its substantially lower pK_a (see above). Figure 6c shows a qualitatively similar pattern for CH_4 as that seen Figure 6b for H_2; however, in the case of CH_4, the partial current is much less sensitive to the anion composition, particularly at low applied potentials, than that for the formation of H_2. We speculate that this difference in sensitivity could be due to the relative importance of surface hydrogenation (via *H) versus hydrogenation from solution (via direct H transfer from liquid-phase H_2O) in the rate-limiting step for the formation of these two products.[42]

3. Conclusions

In this study, we have attempted to develop a complete picture of the role of anion composition on the electrochemical reduction of CO_2. We have confirmed that the composition and concentration of electrolyte anions has relatively little effect on the formation of CO, $HCOO^-$, C_2H_4, and CH_3CH_2OH. This finding is attributed to fact that the rate-limiting step for the formation of each of these products does not involve the addition of hydrogen atoms, a process that can be thought of as the concerted transfer of a proton and electron or the reaction of a water molecule and an electron with the release of a hydroxyl anion. By contrast, the formation of H_2 and CH_4 exhibit a strong sensitivity to the composition and concentration of the electrolyte anion. It is notable that once differences in the pH at the cathode surface versus the bulk electrolyte are taken into account, significant differences in the partial currents for H_2 and CH_4 are still observed at a given potential vs. the RHE (determined using the local pH at the cathode). We propose that these residual differences are associated with the ability of buffering anions to serve as a significant source of hydrogen in competition with water. We note that while the concentrations of buffering anions is much lower than that of water, the pK_a's of these anions are lower than that of water. The results of this study suggest that to maximize the yields of multi-carbon products such as C_2H_4 and CH_3CH_2OH, while minimizing production of H_2 and CH_4, one should use electrolytes with low buffering capacity. While these electrolytes will have a reduced ability to mitigate changes caused by concentration polarization at high reaction rates, which will result in a reduced faradaic efficiency to the desired products, these effects can be offset by reducing the boundary layer thickness for mass transfer by stirring or increasing CO_2 flow rate. In view of the trade-off between the benefits of buffering and non-buffering

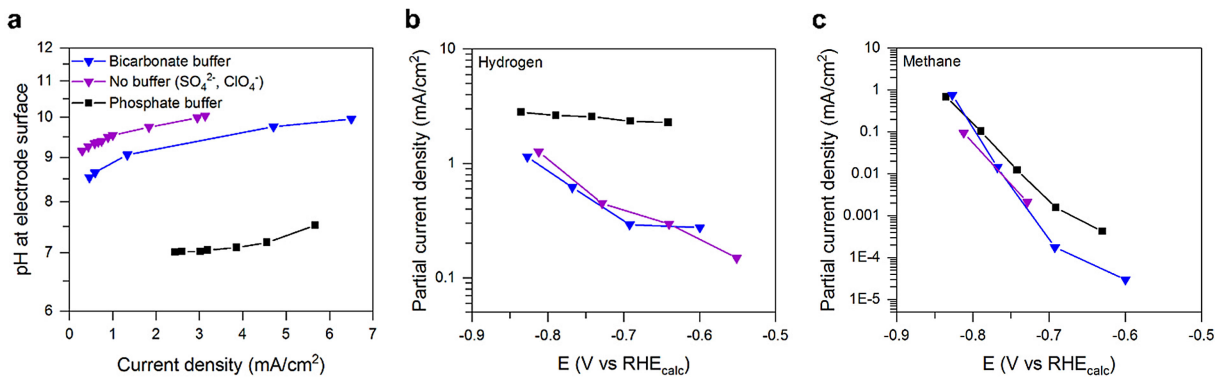

Figure 6. Surface pH and anion identity effects on the partial currents of formation of major products of CO_2 reduction over Cu(100). a) pH at the electrode surface as a function of current density with different anionic electrolytes. All electrolytes are of a fixed potassium cation concentration of 0.1 M. b) Partial current densities for H_2 and CH_4 production as a function of the electrolyte identity on Cu(100). Data are presented at potential between −0.7 and −1.1 V vs. RHE using the calculated local pH, rather than the pH of the bulk electrolyte.

anions, buffering electrolytes of low salinity (0.1 M $KHCO_3$) are preferred to maximize the production of desired C_{2+} products.

Acknowledgement

This material is based upon work performed by the Joint Center for Artificial Photosynthesis, a DOE Energy Innovation Hub, supported through the Office of Science of the U.S. Department of Energy under Award Number DE-SC0004993. J.R. gratefully acknowledges support of the National Science Foundation Graduate Research Fellowship Program (NSF GRFP) under Grant No. DGE-0802270.

Conflict of Interest

The authors declare no conflict of interest.

Keywords: Anion · buffer · CO_2 reduction · copper · electrochemical reduction · electrocatalysis

[1] N. S. Lewis, D. G. Nocera, *Proc. Natl. Acad. Sci.* **2006**, *103*, 15729–15735.
[2] S. Chu, A. Majumdar, *Nature* **2012**, *488*, 294-303.
[3] Y. Hori, H. Wakebe, T. Tsukamoto, O. Koga, *Electrochim. Acta* **1994**, *39*, 1833–1839.
[4] K. P. Kuhl, T. Hatsukade, E. R. Cave, D. N. Abram, J. Kibsgaard, T. F. Jaramillo, *J. Am. Chem. Soc.* **2014**, *136*, 14107–14113.
[5] Y. Hori, In *Modern Aspects of Electrochemistry*, Springer New York, New York, NY, **2008**, pp. 89–189.
[6] K. P. Kuhl, E. R. Cave, D. N. Abram, T. F. Jaramillo, *Energy Environ. Sci.* **2012**, *5*, 7050–7059.
[7] Y. Hori, A. Murata, R. Takahashi, *J. Chem. Soc. Faraday Trans.* **1989**, *85*, 2309–2326.
[8] J. Resasco, L. D. Chen, E. Clark, C. Tsai, C. Hahn, T. F. Jaramillo, K. Chan, A. T. Bell, *J. Am. Chem. Soc.* **2017**, *139*, 11277–11287.
[9] A. S. Varela, M. Kroschel, T. Reier, P. Strasser, *Catal. Today* **2016**, *260*, 8–13.
[10] R. Kas, R. Kortlever, H. Yılmaz, M. T. M. Koper, G. Mul, *ChemElectroChem* **2015**, *2*, 354–358.
[11] S. Zhu, B. Jiang, W.-B. Cai, M. Shao, *J. Am. Chem. Soc.* **2017**, *139*, 15664–15667.
[12] M. Dunwell, Q. Lu, J. M. Heyes, J. Rosen, J. G. Chen, Y. Yan, F. Jiao, B. Xu, *J. Am. Chem. Soc.* **2017**, *139*, 3774–3783.
[13] A. Wuttig, Y. Yoon, J. Ryu, Y. Surendranath, *J. Am. Chem. Soc.* **2017**, *139*, 17109–17113.
[14] C. Hahn, T. Hatsukade, Y.-G. Kim, A. Vailionis, J. H. Baricuatro, D. C. Higgins, S. A. Nitopi, M. P. Soriaga, T. F. Jaramillo, *Proc. Natl. Acad. Sci.* **2017**, *114*, 5918–5923.
[15] H. Jiang, T. J. Klemmer, J. A. Barnard, E. A. Payzant, *J. Vac. Sci. Technol. A* **1998**, *16*, 3376–3383.
[16] Y. G. Kim, J. H. Baricuatro, A. Javier, J. M. Gregoire, M. P. Soriaga, *Langmuir* **2014**, *30*, 15053–15056.
[17] P. Lobaccaro, M. R. Singh, E. L. Clark, Y. Kwon, A. T. Bell, J. W. Ager, *Phys. Chem. Chem. Phys.* **2016**, *18*, 26777–26785.
[18] N. Gupta, M. Gattrell, B. MacDougall, *J. Appl. Electrochem.* **2006**, *36*, 161–172.
[19] J. N. Butler, *Carbon dioxide equilibria and their applications*, CRC Press, **1991**.
[20] W. M. Haynes, *CRC handbook of chemistry and physics*, CRC press, **2014**.
[21] K. G. Schulz, U. Riebesell, B. Rost, S. Thoms, R. E. Zeebe, *Mar. Chem.* **2006**, *100*, 53–65.
[22] Y. Lum, B. Yue, P. Lobaccaro, A. T. Bell, J. W. Ager, *J. Phys. Chem. C* **2017**, *121*, 14191–14203.
[23] Y. Hori, R. Takahashi, Y. Yoshinami, A. Murata, *J. Phys. Chem. B* **1997**, *101*, 7075–7081.
[24] J. D. Goodpaster, A. T. Bell, M. Head-Gordon, *J. Phys. Chem. Lett.* **2016**, *7*, 1471–1477.
[25] J. H. Montoya, C. Shi, K. Chan, J. K. Nørskov, *J. Phys. Chem. Lett.* **2015**, *6*, 2032–2037.
[26] C. Shi, C. P. O'Grady, A. A. Peterson, H. A. Hansen, J. K. Norskov, *Phys. Chem. Chem. Phys.* **2013**, *15*, 7114–7122.
[27] T. Cheng, H. Xiao, W. A. Goddard, *J. Am. Chem. Soc.* **2016**, *138*, 13802–13805.
[28] H. Yoshio, S. Shin, *Bull. Chem. Soc. Jpn.* **1982**, *55*, 660–665.
[29] A. Wuttig, M. Yaguchi, K. Motobayashi, M. Osawa, Y. Surendranath, *Proc. Natl. Acad. Sci.* **2016**, *113*, 4585–4593.
[30] X. Liu, J. Xiao, H. Peng, X. Hong, K. Chan, J.K. Nørskov, *Nat. Commun.* **2017**, *8*, 15438.
[31] M. R. Singh, E. L. Clark, A. T. Bell, *Phys. Chem. Chem. Phys.* **2015**, *17*, 18924–18936.
[32] J. O. M. Bockris, E. C. Potter, *J. Electrochem. Soc.* **1952**, *99*, 169–186.
[33] J. Durst, A. Siebel, C. Simon, F. Hasche, J. Herranz, H. A. Gasteiger, *Energy Environ. Sci.* **2014**, *7*, 2255-2260.
[34] D. Strmcnik, M. Uchimura, C. Wang, R. Subbaraman, N. Danilovic, D. van der Vliet, A. P. Paulikas, V.R. Stamenkovic, N.M. Markovic, *Nat. Chem.* **2013**, *5*, 300–306.
[35] I. Ledezma-Yanez, W. D. Z. Wallace, P. Sebastián-Pascual, V. Climent, J. M. Feliu, M. T. M. Koper, *Nat. Energy* **2017**, *2*, 17031.
[36] W. Sheng, Z. Zhuang, M. Gao, J. Zheng, J. G. Chen, Y. Yan, *Nat. Commun.* **2015**, *6*, 5848.
[37] J. K. Nørskov, T. Bligaard, A. Logadottir, J. R. Kitchin, J. G. Chen, S. Pandelov, U. Stimming, *J. Electrochem. Soc.* **2005**, *152*, 23–26.
[38] A. A. Peterson, F. Abild-Pedersen, F. Studt, J. Rossmeisl, J. K. Norskov, *Energy Environ. Sci.* **2010**, *3*, 1311–1315.
[39] Y. Chen, C. W. Li, M. W. Kanan, *J. Am. Chem. Soc.* **2002**, *134*, 19969–19972.
[40] J. Mostany, E. Herrero, J. M. Feliu, J. Lipkowski, *J. Phys. Chem. B* **2002**, *106*, 12787–12796.
[41] A. Łukomska, J. Sobkowski, *J. Electroanal. Chem.* **2004**, *567*, 95–102.
[42] T. Cheng, H. Xiao, W. A. Goddard, *Proc. Natl. Acad. Sci.* **2017**, *114*, 1795–1800.

Manuscript received: December 8, 2017
Version of record online: February 12, 2018